Structure of Pb2+-deprotonated dGMP complexes in the gas phase: a combined MS-MS/IRMPD spectroscopy/Ion Mobility study

Jean-Yves Salpin, Luke Macaleese, Fabien Chirot, Philippe Dugourd

Structure of Pb^{2+}/deprotonated dGMP complexes in the gas phase: a combined MS-MS/IRMPD spectroscopy/Ion Mobility study.

Jean-Yves Salpin[1,2], *Luke MacAleese*[3,4], *Fabien Chirot*[5,6], *Philippe Dugourd*[3,4,]

1) Université d'Evry Val d'Essonne – Laboratoire Analyse et Modélisation pour la Biologie et l'Environnement – Boulevard François Mitterrand – 91025 Evry – France
2) CNRS- UMR 8587.

3) Université Lyon 1– Institut Lumière Matière, 5 rue de la Doua, 69622 Villeurbanne cedex, France

4) CNRS- UMR 5306.

5) Université Lyon 1 – Institut des Sciences Analytiques, 5 rue de la Doua, 69100 Villeurbanne– France

6) CNRS- UMR 5280

Corresponding authors:

Dr Jean-Yves Salpin
e-mail: jean-yves.salpin@univ-evry.fr

Dr Luke MacAleese
e-mail: luke.macaleese@univ-lyon1.fr

Abstract

The structure of the Pb^{2+}/ deprotonated deoxyguanosine-5'-monophosphate (dGMP) complex, generated in the gas-phase by electrospray ionization, was examined by combining tandem mass spectrometry, mid-infrared multiple-photon dissociation (IRMPD) spectroscopy and ion mobility. In the gas phase, the main binding site of Pb^{2+} onto dGMP is the deprotonated phosphate group, but the question is whether an additional stabilization of the metallic complex can occur via participation of the carbonyl group of guanine. Such macrochelates indeed correspond to the most stable structures according to theoretical calculations. A multiplexed experimental approach was used to characterize the gas-phase conformation of the metallic complex and hence determine the binding mode of Pb^{2+} with $dGMP^{-}$. MS/MS analysis observation of characteristic bands by IRMPD spectroscopy and measurement of ion mobility collision cross section suggest that gaseous $[Pb(dGMP)-H]^{+}$ complexes adopt a macrochelate folded structure, which consequently differs strongly from the zwitterionic forms postulated in solution from potentiometric studies.

I-Introduction

Since its discovery in the beginning of the 20th century, mass spectrometry has become one of the most powerful analytical methods, more especially with the advent of soft ionization methods, which allow intact biomolecules to be easily ionized and transferred into the gas phase. Structural characterization of biopolymers such as peptides, oligosaccharides and oligonucleotides is mostly achieved by tandem mass spectrometry methods (MS/MS) based upon the activation of precursor ions by collisions with a buffer gas. Collision induced dissociation (CID) experiments indeed provide invaluable data regarding the primary sequence of these biomolecules. More recently, alternate activation methods such as electron capture dissociation (ECD)[1], electron transfer dissociation (ETD)[1, 2], electron detachment dissociation (EDD)[3] or electron photodetachement dissociation (EPD)[4], demonstrated to provide complementary sequences information in comparison to CID, due to different dissociation mechanisms, thereby leading to increased peptide sequence coverage.

Although particularly useful, these methods hardly provide any information about the spatial arrangement of ions in the gas phase. To address this question, several instrumental approaches have emerged during the last decade. Coupled with mass spectrometry, these setups offer value-added data that cannot be obtained by mass spectrometry alone. Among those approaches, ion mobility spectrometry (IMS) is an analytical technique used to separate and characterize ionized molecules in the gas phase based on their mobility in a buffer gas, under the influence of an electric field. It allows isomer separation, and provides global insight in ions conformation through the measurement of their collision cross section (CCS) in the buffer gas. [5-10] Complementary and strongly structure-sensitive technique is infrared (IR) multiple photon dissociation (IR-MPD). [11, 12] This spectroscopic technique is often termed “action spectroscopy” since resonant IR absorption cannot be directly probed due to the low ion density within a mass spectrometer. Nevertheless, provided the use of intense and tunable infrared sources such as free electron lasers, ion fragmentation can be induced by a multiple-photon absorption process, and fragment ions can be mass-analyzed as a function of the photon energy. Detailed analysis of spectral features can yield information on the local molecular arrangement,

especially regarding the H-bonds network. In many cases, results from one of the above techniques alone are not sufficient to unambiguously assign a structure to a complex molecular system. A fruitful approach thus consists in gathering the local conformational data from IRMPD, and the global information on molecular shape yield by IMS. Such coupled approach also has advantages regarding the interpretation of the experimental results. For both techniques, it relies on comparison with molecular simulations on candidate structures.

Structural studies combining ion mobility and action spectroscopy are rather scarce in the literature, and for now were devoted to structural characterization of ionized amino acids [13], peptides[14-17] or sugars.[18] In the present work, as part of our ongoing effort to describe the interactions occurring in the gas phase between divalent metal ions and DNA building blocks[19-26], we combined IMS, IRMPD and MS/MS experiments with theoretical calculations in order to characterize the structure of complexes generated in the gas phase between Pb^{2+} and 2′-deoxyguanosine-5′-monophosphate (dGMP, scheme 1). In the gas phase, the main binding site of Pb^{2+} with mononucleotides is the deprotonated phosphate group[23, 24], but the question is whether an additional stabilization of the metallic complex can occur via participation of the carbonyl group of the nucleobase.

The present strategy allowed us obtaining a complete set of complementary data, thereby allowing very detailed structural characterization and comparison with data determined in solution for such systems.

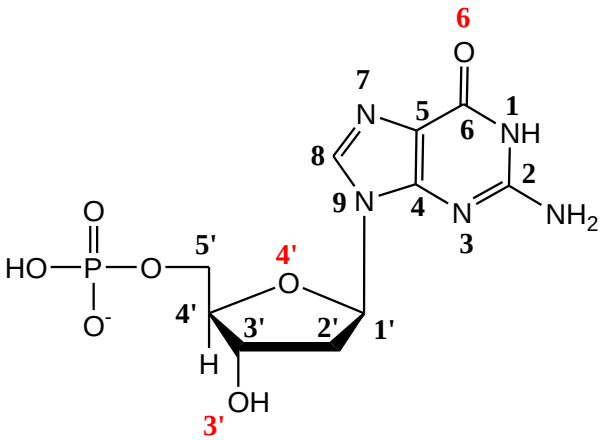

Scheme 1

2-Methodology

(a) Materials

Lead nitrate $(PbNO_3)_2$ and dGMP used in this work were research grade products from commercial sources (Sigma-Aldrich, Saint Quentin Fallavier, France) and were used without any further purification. Stock aqueous solutions of lead nitrate and nucleotide were prepared at 10^{-2}M by using purified water (purified with a Milli-Q water purification system, resulting pH 5.5). Lead nitrate/dGMP mixtures were then diluted at various concentrations and ratios, in a water/methanol mixture (50/50 v/v), prior to their introduction into electrospray sources.

(b) Tandem-Mass spectrometry experiments

Electrospray mass spectra were recorded on an Applied Biosystems/MDS Sciex API2000 triple-quadrupole instrument fitted with a "turboionspray" ion source. Solutions of lead nitrate/dGMP, were introduced in the source using direct infusion with a syringe pump, at a flow rate of 5 µl/min. Ionization of the samples was achieved by applying a voltage of 4.0 kV on the sprayer probe, and by the use of a nebulizing gas (GAS1, air) surrounding the sprayer probe, intersected by a heated gas (GAS2, air) at an angle of approximately 90°. The operating pressure of GAS1 and GAS2 are adjusted to 2.1 Bar, while the curtain gas (N2), 1.4 Bar. The temperature of GAS2 was set at 100°C. The difference of potentials between the orifice plate and the skimmer (declustering potential, DP), ranged from 20 to 80 V to perform the various experiments.

MS/MS spectra were systematically recorded at various collision energies ranging from 0 eV to 30 eV in the laboratory frame (the collision energy is given by the difference between the potentials of Q0 and Q2). The CAD parameter controlling the amount of N_2 introduced into Q2 was set to its minimum value in order to limit multiple ion–molecule collisions.

Unless otherwise noted, Mass to charge ratios mentioned throughout this paper refer to peaks including the most abundant lead isotope (^{208}Pb).

(c) IRMPD spectroscopy experiments

The present IRMPD study has been performed using a Fourier transform–ion cyclotron resonance (FT-ICR) instrument into which pulsed IR light is coupled.[27] This particular experimental setup has already been described in details elsewhere.[27] The most important feature for the present study is the quadrupole-hexapole interface between the electrospray source and the ICR cell. The bias voltage and RF amplitude of the quadrupole are adjusted to selectively transmit $[Pb(dGMP)-H]^+$ complexes. Mass-selected ions are then trapped in a ~5 cm long hexapole ion trap contained within a collision cell where ions are collisionally cooled using a flow of high-purity argon buffer gas. Ions are then pulse-extracted towards the ICR cell where mass-selection of the complexes is performed. They are then irradiated with IR light, after which the resulting ions are mass-analyzed. $[Pb(dGMP)-H]^+$ complexes were prepared in an electrospray source (ESI) source by direct infusion of equimolar lead nitrate/dGMP mixtures (10^{-4}M, water/methanol 50/50 v/v). ESI conditions used are a flow rate of 3µl/min, a spray voltage of 3500 V and a capillary temperature of 200°C.

IR spectroscopy was performed using the CLIO (centre laser infrarouge d'Orsay) free electron laser (FEL), which produces pulsed, tunable IR light covering the 100-2500 cm^{-1} wavenumber range.[28] The light is produced in an 8 µs long pulse train, the macropulse, of IR laser pulses a few picoseconds in duration, the micropulses. The macropulse repetition rate is 25 Hz while that of the micropulse is 62.5 MHz. Using electron energy of 45 MeV, IRMPD spectra could be recorded over the 1000-2000 cm^{-1} energy range.

If the IR light is in resonance with an IR active vibrational mode of molecular ions stored in the ICR cell, IR photons can be absorbed and the sequential absorption of several IR photons can lead to fragmentation of the mass-selected ions. This photo-fragmentation, which is the result of a multiple photon absorption process, is often termed infrared multiple photon dissociation (IRMPD). In the present case, it can be noticed that only one or two macropulses were sufficient to achieve high photo-fragmentation yields (irradiation time 50-100 ms). At each wavelength, the mass spectrum is the Fourier transform of a time-domain transient averaged 5 times. The IRMPD spectrum is obtained by

plotting the photofragmentation yield R ($R = -\ln[I_{parent}/(I_{parent} + \Sigma I_{fragment})]$ where I_{parent} and $I_{fragment}$ are the integrated intensities of the mass peaks of the precursor and of the fragment ions, respectively) as a function of the frequency of the IR radiation.[29] A recent study[30] has demonstrated that this data treatment allows a better comparison between IRMPD intensities and calculated infrared absorption spectra and a better spectral resolution than other analysis methods.

(d) Ion Mobility experiments

Ion mobility mass spectrometry (IM-MS) measurements were performed on a custom-built ion mobility spectrometer first described elsewhere. [31] Briefly, a 1 m-long drift tube is inserted between the electrospray ion source and the ion transfer part of a commercial Q-TOF mass spectrometer (microToFQ, Bruker-Daltonics, Bremen, Germany). Ions formed in the ESI source are trapped and accumulated ahead of the drift tube in an hourglass-shaped funnel ion trap. Short ion bunches (800 µs) are injected into the tube at a repetition rate of ~5Hz. A Helium pressure of 12.8 Torr is maintained in the tube, and the temperature of the whole setup is kept at 296K, the regulated temperature of the experimental room. Drift fields ranging from 300 to 1000 $V.m^{-1}$ can be used for measurements. Ions exiting the drift tube are finally collected via a series of 3 ion-funnels and guided through the Q-TOF instrument in which two detection modes are available. Time of flight (TOF) mass spectra can be recorded as a function of the ion mobility drift time (IMS) to yield high resolution IMS-MS measurements which allows accurate comparison between the drift times of species with different *m/z* ratios. When the mass spectrum of the sample solution is sufficiently not congested so that the ion of interest can be efficiently mass-selected in the q-TOF quadrupole (which is the case in the present study), arrival time distributions can be recorded directly from the dynode detector by turning off the push-pull voltages of the orthogonal TOF. Even if mass-resolution is lower in this latter mode, it offers a much higher sensitivity.

The determination of collision cross section (CCS) for an ion relies on the measurement of its IMS drift time t_d as a function of the drift voltage. In the experimental conditions, the movement of an ion

of mass M and charge q in the drift tube falls in the so-called low-field ion mobility regime.[32] Its drift time across the tube then depends on the buffer gas mass m, temperature T, and pressure p, and on the applied electric field E. It is related to the collision cross section Ω (more rigorously the rotationally-averaged momentum transfer cross section in ion-buffer gas collisions) through[32]:

$$t_d = \frac{16}{3}\sqrt{\frac{\mu}{2\pi k_B T}}\frac{p}{q}\frac{L}{E}\,\Omega$$

, where $\mu = \frac{Mm}{m+M}$ is the reduced mass, and k_B is the Boltzmann constant.

The time that is actually measured in an IMS experiment is $t_{mes} = t_d + t_0$, t_0 being the time necessary for an ion to travel from the end of the drift region to the detector. The most accurate way to measure Ω, is then to plot t_{mes} against the inverse voltage and to perform a linear regression on the recorded data (see Supporting Information). The value of Ω is finally extracted from the slope, the intercept being t_0.

In the present case, trapping voltages are adjusted to optimize the $[Pb(dGMP)-H]^+$ ion signal intensity. $[Pb(dGMP)-H]^+$ ions are selected at *m/z* 554±5 with the quadrupole mass filter. Selected ions are injected with a very low energy (2 eV) in the collision cell (gas flow 20% in Bruker control software) and their arrival time is monitored directly from the dynode on a scope. Drift field is varied from 400V/m to 850V/m by steps of 50V/m and $[Pb(dGMP)-H]^+$ ion arrival time is measured repeatedly up to 4 times per drift field value (see section 5S of the Supporting information).

(e) Theoretical calculations

Molecular orbital calculations were carried out using the B3LYP density functional, as implemented in the Gaussian-03 set of programs [33]. B3LYP combines the non-local correlation function of Lee, Yang and Parr [34], with the Becke's three-parameter non-local hybrid exchange functional [35]. In a first step, the different structures were optimized with the dp-polarized 6-31G(d,p) basis, without any symmetry constraint. We used for Pb the "Stuttgart" quasi-relativistic pseudo-potential developed by

Küchle *et al.*[36]. This particular 78-electrons effective core potential (ECP) employs a (4s,4p,1d)/[2s,2p,1d] basis set with a (3,1) contraction scheme for s and p functions that can be used directly in conjunction with the standard 6-31G(d,p) Pople basis set describing C, N, O, P and H atoms. Harmonic vibrational frequencies were estimated at this level to classify the stationary points as local minima or saddle points, and to estimate the zero-point vibrational energy (ZPE) corrections. Provided the use of an appropriate scaling factor, hybrid DFT methods such as B3LYP have been shown to outperform other DFT methods as well as traditional *ab initio* approaches to describe both position [37] and relative intensities [38] of IR bands. With regards to band positions, a scaling factor value of 0.96 has been chosen on the basis of the overall good agreement between experimental and computed frequencies for a large set of molecules.[39] Finally, for ease of comparison with the experimental spectrum, calculated spectra were convoluted with a 15 cm^{-1} fwhm Gaussian function. Relative energies were refined at the 6-311+G(2df,2p) level, by using for lead a self-developed 6-311+G(2df) basis set. We demonstrated that this basis set, in combination with the B3LYP functional, provides a good compromise between accuracy and computational cost for energy calculations. [40] Throughout this paper relative free energies are expressed in kJ/mol. For sake of simplicity, Pb-basis sets will be referred to as 6-31G(d,p) and 6-311+G(2df,2p) basis sets. Detailed geometries of all structures mentioned in this paper are available from authors upon request.

In order to compare the results of the calculations to IMS experimental results, theoretical collision cross sections (CCS) were also calculated for candidate structures using an exact hard-sphere scattering (EHSS) model[41] and the projection approximation (PA)[42, 43]. Since lead and phosphorus are not originally parameterized in the model, and since the trajectory method developed by Mesleh *et al.* [44]requires additional parameters more difficult to evaluate than hard-sphere radii, only PA and EHSS approaches were used in this study. Although those methods are not as accurate as the Trajectory method [41,42] or the projected superposition approximation[45], they provide orders of magnitude that prove very useful in comparing families of conformations. Hard-sphere radii had to be adjusted: from literature[46] atomic radii of P and Pb^{2+} are respectively 110 pm and 120pm, both comparable to Si

radius (115pm). As a result, Si parameters (from M.F. Jarrold's MOBCAL program) are taken to model both P and Pb^{2+}. Variability in CCS arising from this hypothesis was evaluated by carrying out calculations with hard sphere radii of P and Pb^{2+} varied by + (respectively -) 20% of the tabulated value for Si. Resulting CCSs increase by ~2-7A^2 (respectively decrease by 2-4A^2) with an expected larger effect for unfolded structures. However, those differences are consistent among different structures and methods, and the CCS gap between folded and unfolded structures remains large and significant. The "Si approximation" can therefore be considered sound and reasonable.

3-Results/discussion

3.1 Mass spectrometry.

During sample preparation, dGMP is dissolved in purified water with pH 5.5. At this pH value, mononucleotides (XMP) are singly deprotonated and interaction with Pb^{2+} cation results in the formation of $[Pb(XMP)-H]^+$ complexes. [47] Logically, electrospraying a 1:1 mixture (10^{-4} M) of lead nitrate and dGMP results in the formation of abundant $[Pb(dGMP)-H]^+$ complexes (*m/z* 554). However, regardless of the interface conditions, this species does not correspond to the base peak, due to competitive interaction between the metal and the solvents. At low DP values, the most prominent ions are indeed lead hydroxide $PbOH^+$ (*m/z* 225) and $PbOCH_3^+$ (*m/z* 239). When increasing the declustering potential, these two ions quickly disappear and a slow decay of the lead/nucleotide complex is observed. Finally, at high cone voltage (DP> 120V), the electrospray spectrum is dominated by Pb^+ (*m/z* 208) and PbH^+ ions (*m/z* 209). Other species such as protonated guanine (*m/z* 152) and protonated dGMP (*m/z* 348) are also detected with significant abundance. No doubly charged ions were detected during these experiments.

The MS/MS study was initiated by first recording the MS/MS spectrum of the $[Pb(dGMP)-H]^+$, in order to characterize its fragment ions (Figure 1). We then observed that increasing the DP parameter allows fragment ions of the $[Pb(dGMP)-H]^+$ complex to be also detected on the ESI spectrum (in-source fragmentation). So, we opted for a DP value of 40 V to induce in-source fragmentation. Then,

each fragment ion thus generated was selected individually by the first quadrupole to record its MS/MS spectrum. The whole set of MS/MS data led to the dissociation pattern summarized in Scheme 2.

The CID spectrum obtained for $[Pb(dGMP)-H]^+$ at 25 eV (laboratory frame) is given in Figure 1. This spectrum does not depend on the DP parameter

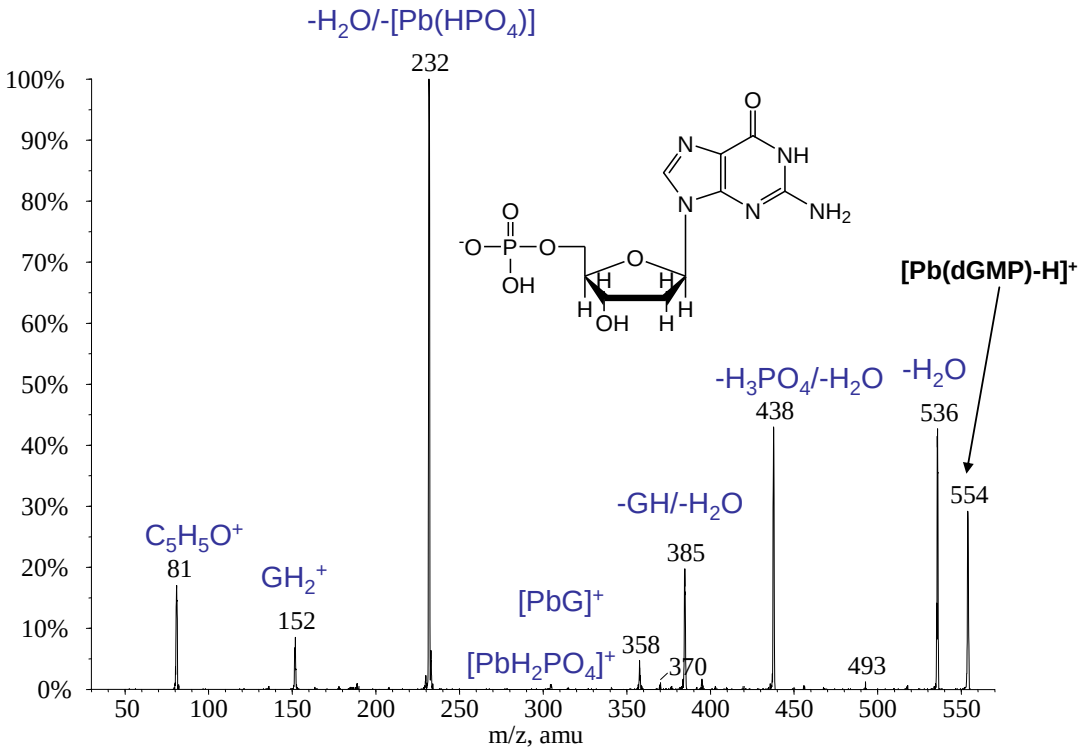

Figure 1: MS/MS spectrum of the $[Pb(dGMP)-H]^+$ complex recorded with a collision energy of 25 eV (laboratory frame) and a DP parameter set to 40 V.

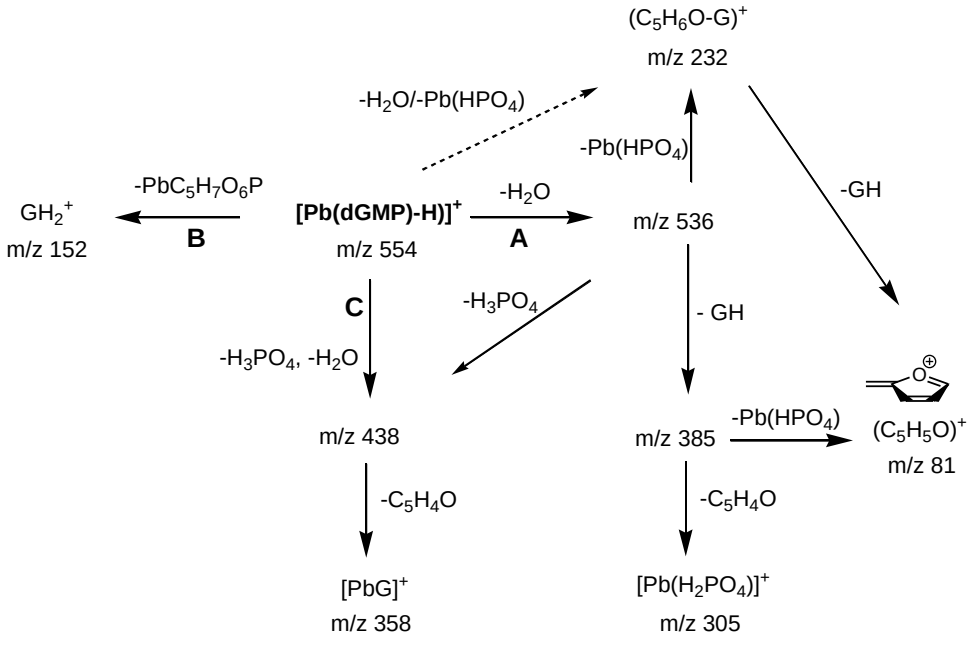

Scheme 2

Starting from the $[Pb(dGMP)-H]^+$ precursor ion, three main processes are observed. The first one (**A**) corresponds to dehydration associated with the formation of the *m/z* 536 ion, which further expels the nucleobase (GH) to generate the *m/z* 385 species. This particular sequence has already been observed for other $[Pb(XMP)-H]^+$ ions (XMP=UMP[24], CMP[23], dCMP[23]), and also for Cat^+/TMP complexes (Cat=Li, Na, Cs)[48, 49]. The latter species then dissociates according to two processes, associated either with the loss of the sugar moiety ($-C_5H_4O$) and formation of $[PbH_2PO_4]^+$ (*m/z* 305), or to the elimination of $PbHPO_4$ giving rise to $C_5H_5O^+$ (*m/z* 81). The latter fragment is very likely a sugar-derived species (scheme 2) as deduced previously from deuterium exchange experiments.[50] These two fragment ions strongly suggest that the metallic center interacts with the phosphate group. Loss of $PbHPO_4$ is also observed from *m/z* 536 ion, leading to *m/z* 232 ion which can be assigned to $(C_5H_6O-G)^+$ as it further dissociates by loss of neutral guanine to generate $C_5H_5O^+$ (*m/z* 81).

The second dissociation channel (**B**) experienced by the initial complex is the formation of the protonated nucleobase (GH_2^+) detected at *m/z* 152. Its intensity in the MS/MS spectra is rather weak. Note that direct elimination of neutral guanine is presently not observed, while it is detected in significant abundance for the $[Pb(GMP)-H]^+$ complex (see Figure 1S of the Supporting Information). As already shown in a previous study[23], direct elimination of either neutral or protonated nucleobase is more pronounced in the case of ribo-mononucleotides, suggesting that the 2' hydroxyl group might play an important role in these fragmentation processes.

These two first dissociation pathways rather suggest the interaction of the metallic center with the phosphate moiety of dGMP. These findings are not in agreement with the structure of the complexes formed in solution between Pb^{2+} and GMP. Indeed, the potentiometric studies carried out by Sigel and co-workers [51, 52] suggest that Pb^{2+} ions should mostly interact with the guanine moiety. On the other hand, the third dissociation route (**C**) leading ultimately to the $[PbG]^+$ ion (*m/z* 358), indicates that within the complex, Pb^{2+} may also interact with the nucleobase. MS/MS data therefore suggest that several coordination modes might coexist in the gas phase. Consequently, in order to complete

MS/MS data, quantum chemical calculations as well as complementary experimental approaches (ion mobility and IRMPD spectroscopy) have been carried out.

3.2 Theoretical calculations.

Mononucleotides are quite flexible molecules, and consequently performing a complete conformational survey is challenging. However, based on i) our previous studies on pyrimidic nucleobases[19] and mononucleotides[23, 24], which have shown the strong affinity of lead for carbonyl groups, and ii) the fact that the phosphate group is at least singly deprotonated under our experimental conditions, we limited the number of starting geometries. Zwitterionic forms (with the metal located away from the deprotonated phosphate group) were considered since they have been postulated as the mains forms in solution for $Pb^{2+}/(GMP\text{-}H)^-$ complexes, according to potentiometric studies.[51, 52] In addition, we also considered the possibility of a doubly-deprotonated phosphate group since elimination of neutral [$Pb(HPO_4)$] is observed experimentally.

Representative structures obtained for $[Pb(dGMP)\text{-}H]^+$ complexes, are presented in Figure 2 while their relative free energies. are summarized Table 1. The various forms are labeled according to the *Syn* or *Anti* orientation of the nucleobase. Detailed description of all the forms investigated (coordination mode, ring puckering, base orientation, internal hydrogen bonding) is provided in the section 2S of the supporting information. Relative free energies of all the forms (except **dGMPA10** and **dGMPS1** which did not converge) were refined at the B3LYP/6-311+G(2df,2p). A slight variation in relative free energies is observed when increasing the level of calculation. One noticeable effect is the narrowing in the energy gap for the three most stable species.

We located stable (positive eigenvalue) zwitterionic forms both with *Anti* (**dGMPA1**) and *Syn* oriented (**dGMPS1**) nucleobase. However, these forms are located at about 370 kJ/mol above the global minimum (Table 1), and consequently are not likely to be generated in the gas phase. We also optimized a series of structures for which the metal interacts with a doubly deprotonated phosphate group and the guanine residue is protonated. For *Anti* forms (**dGMPA2-7**), we considered three

distinct protonation sites, namely, N7, O6 and N3 (scheme 1). Comparison between **dGMPA2** and **dGMPA3** shows that interaction with the carbonyl group of the guanine residue (**dGMPA3**) does not provide any significant stabilization. Examination of Table 1 indicates that the energy order follows the relative proton affinity order of these three sites [53-55], N7-protonated forms being sensibly more stable (~58 kJ/mol) for *Anti* structures. Consequently, for *Syn* structures only protonation onto N7 was considered (**dGMPS2**).

All the doubly-deprotonated forms correspond to minima on the potential energy surface and are considerably more stable than the zwitterions. N7-protonated forms indeed are about 280-300 kJ/mol lower in relative free energies than zwitterions, but still 74-120 kJ/mol above the global minimum (**dGMPS10**).

Anti forms

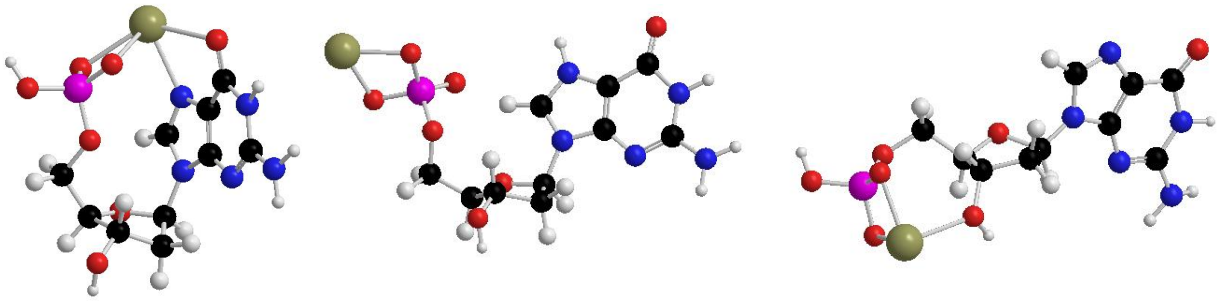

dGMPA13 +1.8 **dGMPA2 +74.3** **dGMPA12 +125.9**

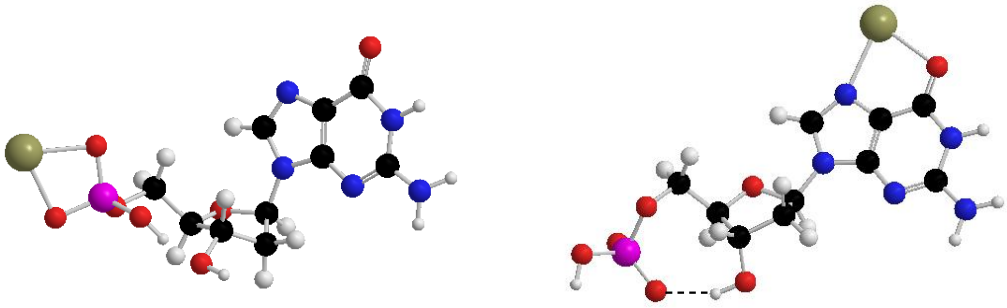

dGMPA9 +147.3 **dGMPA1 +366.7**

Syn forms

dGMPS10 0.0 **dGMPS9 +9.5**

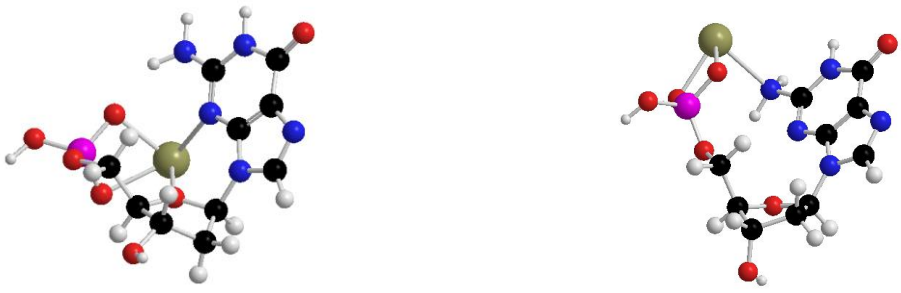

dGMPS7 + 85.0 **dGMPS5 +161.5**

Figure 2: Representative optimized structures of the $[Pb(dGMP)-H]^+$ complex. Relative free energies are given in kJ/mol.

With our sample preparation conditions, dGMP should be singly deprotonated in water, and we therefore concentrated our efforts onto structures involving singly deprotonated nucleotide. These structures can be classified into two groups. The first group includes forms in which the metallic center only interacts with the phosphate moiety (**dGMPA8-12 and dGMPS3-4**). All these forms are found more stable than the zwitterionic structures, therefore suggesting that unlike in solution[51], the metal exhibits a much stronger affinity for the singly-deprotonated phosphate group than for the nucleobase. Like for dCMP [23], the most favorable coordination scheme is characterized by a metal interacting with two oxygen atoms of the phosphate group and the O3'H hydroxyl group (**dGMPA11-12**/**dGMPS4**). The other binding mode (**dGMPA10**) involving the phosphate hydroxyl group appears much less favorable (Table 1). This finding is consistent with previous studies[19, 22], which demonstrated the poor affinity of lead for OH groups in the gas phase.

The second group of structures, denoted as macrochelates, is characterized by a metal interacting not only with the phosphate moiety, but also with the guanine residue. Unlike doubly deprotonated forms (**dGMPA2**), additional interaction with the nucleobase results in strong structural stabilization. Different types of macrochelates were obtained. The most stable coordination mode is characterized by a tetradentate interaction involving two oxygens of the phosphate group, N7 and the carbonyl group of the guanine residue. Both *Syn* and *Anti* forms were obtained, although optimization of the former turned to be easier. They exhibit very similar stabilities, the global minimum being **dGMPS10**. The two additional interactions with the guanine residue provide a very important stabilization, macrochelates being at least 126 kJ/mol more stable than the unfolded structures of the first group (**dGMPS4**). Other binding schemes were optimized, notably involving N3 (**dGMPS6**) or the amino group (**dGMPS5**), but they appear sensibly less stable. Interaction with a single phosphate oxygen (**dGMPS6** and **dGMPS8**) also results in less stable forms. Within macrochelates, interaction with the carbonyl group is more pronounced in case of tridentate binding scheme (**dGMPS8**) than for tetradentate coordination mode (**dGMPA13/dGMPS9/dGMPS10**), as attested by the more important bond lengthening (1.263 Å and 1.247 Å, respectively), compared to the value typically obtained at this

level of calculation for free carbonyls (1.210 Å). Interaction with the nucleobase is also characterized by a small distortion of the purine moiety from planarity (typical values for the N7C5C4C6 torsional angle being of 165-166°). This distortion effect is less pronounced (178°) when the metal interacts with N3 (**dGMPS6** and **dGMPS7**). Finally, interaction with the endocyclic O4' oxygen (**dGMPS6**/**dGMPS7**) atom has also been considered, but has no positive effect onto the stability of the complex.

In summary, from calculations three near iso-energetic structures are found to be particularly stable: **dGMPA13**, **dGMPS9** and **dGMPS10**. These three forms correspond to macrochelates involving a tetradentate coordination of Pb^{2+}, and are therefore very different from those present in solution (zwitterions).

3.3 IRMPD spectroscopy

In order to get more insights, we performed IRMPD spectroscopy experiments. IRMPD spectroscopy has been widely applied to characterize the structure of metal-cationized complexes [12], and notably of metal/DNA blocks species [23, 24, 26, 56, 57]. In the current work, IRMPD spectra have been recorded in the 1000-1900 cm^{-1} energy range. On resonance with an infrared active mode of the mass-selected $[Pb(dGMP)-H]^+$ complex, two photo-fragments are observed, a particularly intense dehydration (*m/z* 536) together with combined elimination of water plus phosphoric acid (*m/z* 438). The fragmentation scheme was similar for $[Pb(dCMP)-H]^+$ [23]. The experimental optical spectrum presently reported was obtained by considering the two photo-fragments.

The IRMPD spectrum of the $[Pb(dGMP)-H]^+$ ion is given in Figure 3a. The assignment of the IRMPD spectrum is based on its comparison with spectra computed for various low-energy isomers. The vibrational bands computed for quasi-degenerated **dGMPA13** and **dGMPS10** forms, are summarized in Table 2. In making these comparisons, one should keep in mind that the calculated IR intensities, which assume single photon absorption, often do not correspond well with the multiple photon spectrum, because of the complex nature of the IRMPD process [29, 58, 59].

The IRMPD spectrum of the $[Pb(dGMP)-H]^+$ complex features a very broad band (fwhm~120 cm^{-1}) centered at 1080 cm^{-1}. As already established from the comparison between the IRMPD spectra of $[Pb(UMP)-H]^+$ and $[Pb(Urd)-H]^+$ complexes[24] (UMP and Urd stand for Uridine-5'-monophosphate and Uridine, respectively), this broad feature corresponds to IR-active modes of the phosphate group. A shoulder is observed around 1110 cm^{-1}, suggesting that this signal corresponds to at least the convolution of two IR-active modes, since with this particular experimental setup, isolated IR-active vibrational modes generally give rise to IRMPD bands of of 10-20 cm^{-1} width .[27] This is also consistent with the numerous vibrational modes (notably P-O and C'-O' stretches, P–O–H bending mode) computed in this energy range (Table 2). Two smaller but significant bands are detected at about 1180 and 1325 cm^{-1}. A weak band is also detected at about 1390 cm^{-1}. Finally, the high-energy region above 1500 cm^{-1} is characterized by three strong and sharp partially coalescing features, detected at 1586, 1625 and 1670 cm^{-1}. As guanine residue presents a carbonyl group, the C=O stretching mode constitutes an excellent infrared diagnostic to determine whether the metallic center interacts with this particular group. Figures 3e and 3f show the DFT-calculated IR absorption spectrum of **dGMPA12** and **dGMPA2**, in which the metal solely interacts with the phosphate group. These two forms exhibit strong transitions at 1774 and 1768 cm^{-1}, respectively, corresponding to the free C6=O6 stretching mode. Experimentally, there is no signal above 1700 cm^{-1}, unlike what was observed for $[Pb(UMP)-H]^+$ complex.[24] In addition, these two spectra do not account for the strong experimental feature measured at 1670 cm^{-1}. Consequently, gas-phase structures characterized by a lead atom interacting solely with the phosphate group (including zwitterionic forms, see Supporting Information, section 4S) can be reasonably ruled out. This also suggests that such structures, postulated in solution[51, 52] for the $Pb^{2+}/(GMP-H)^-$ system, are not stable in the gas phase. Conversely, a very good agreement is observed between the experimental spectrum and the IR spectrum of the global minimum **dGMPS10** as well as low energy forms **dGMPS9** and **dGMPA13**. The spectrum of

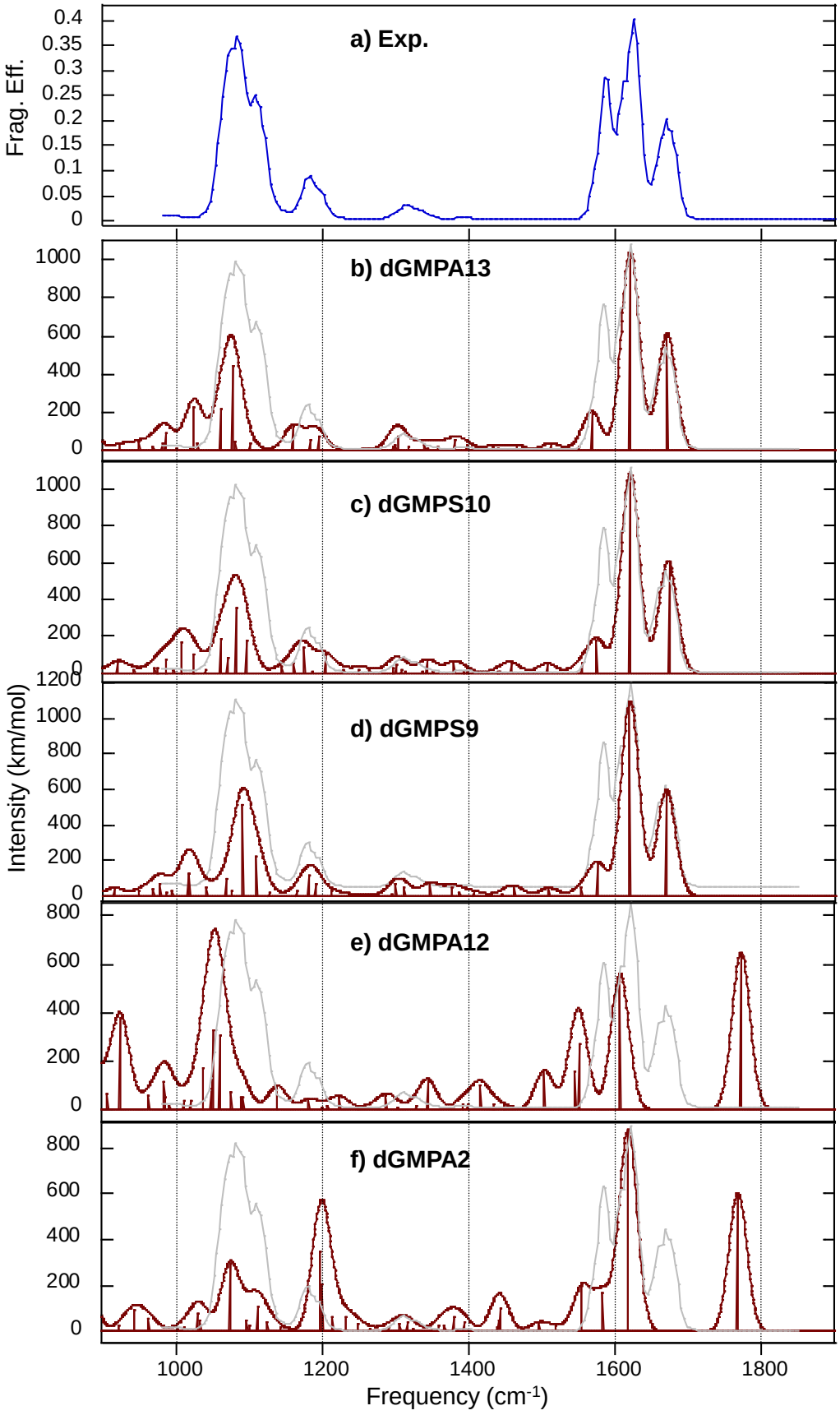

Figure 3: IRMPD spectrum (a) obtained for the $[Pb(dGMP)-H]^+$ complex compared to DFT-computed IR absorption spectra (b–f) of some relevant structures. The experimental IRPMD spectrum in overlayed in grey.

dGMPS10 exhibits three strong IR active modes lying in the 1000-1100 cm^{-1} energy range, which may account for the very broad band observed experimentally. Examination of table 2 indicates that the broad feature centered at 1080 cm^{-1} may correspond to combined C'–O' and P-O stretching modes, as well as P-O-H bending mode. One particularly important finding is the excellent agreement in terms of position between the experimental signal and the computed frequencies above 1500 cm^{-1}. First, the sharp signal detected at 1586 cm^{-1} may be attributed to the C4-C5 stretching mode. According to Table 2, the band at 1625 cm^{-1} may correspond to the NH_2 scissoring mode. Finally, the band observed at high energy (1670 cm^{-1}), is consistent with the C6=O6 stretching mode. This CO stretch is therefore red-shifted by ~100 cm^{-1} with respect to **dGMPA2** or **dGMPA12**, and is a signature of an interaction taking place between the metal and the guanine carbonyl group, resulting in the C6=O6 bond lengthening. However, this red-shift is markedly less pronounced than those observed for $[Pb(UMP)-H]^+$ and $[Pb(dCMP)-H]^+$ ions (>150 cm^{-1}), suggesting a weaker Pb/C=O interaction with the guanine residue. Accordingly, the computed bond length for the interacting C=O is shorter for guanine (1.247 Å) than for cytosine (1.275 Å[23]) or uracil (1.277 [24]). This weaker interaction partly explains why the IRMPD signature of the $[Pb(dGMP)-H]^+$ complex above 1400 wavenumbers differs from those recorded for $[Pb(dCMP)-H]^+$, $[Pb(CMP)-H]^+$[23] or $[Pb(UMP)-H]^+$[24], the C=O stretch of the interacting carbonyl group being located between 1556 and 1586 cm^{-1} for the three latters. Note also that the IRMPD spectrum of $[Pb(dGMP)-H]^+$ is devoid of any strong feature around 1480 cm^{-1}, which was notably characteristic of the presence of a tautomer for $[Pb(UMP)-H]^+$ [24].

The three remaining experimental signals are also in agreement with computed vibrational modes of the three most stable forms (**dGMPS10**, **dGMPS9**, **dGMPA13)**. Experimental bands detected around 1180 and 1325 cm^{-1} could be attributed to combined C'–O'–H and C'–C'–H bending modes and combined C–N–H and C'–C'–H bending modes, respectively. Finally, the small signal detected around 1390 cm^{-1} may also be interpreted (Table 2). On the other hand, several modes expected at 1025 cm^{-1} and between 1400 and 1550 wavenumbers are not observed experimentally. It has been previously

observed that small absorptions may be missing in IRMPD spectra.[60-63] Possible reasons lie in the multiphotonic nature of IRMPD and the requisite efficiency of intramolecular vibrational redistribution.

Interestingly, macrochelates such as **dGMPS10** (Figure 3c), **dGMPS9** (Figure 3d), or **dGMPA13** (Figure 3a), differing by the nucleobase orientation but sharing the same binding scheme and the same ring puckering, lead to a very good agreement with the experimental trace. Computed spectra for these forms are indeed very similar. Consequently, such slight structural differences can be delicate to distinguish by IRMPD and the formation in the gas phase of a mixture of several macrochelate forms appears very likely.

Figure 4S displays the computed spectrum of **dGMPA3**, which is a macrochelate form exhibiting a doubly deprotonated phosphate group. This spectrum differs from the experimental trace in several aspects and notably in the high energy region, where the computed energy gap between the two most active modes (30 cm^{-1}) does not reproduce the gap observed experimentally (45 cm^{-1}) signal. Additionally, one would expect bands with sensibly comparable intensities at 1080 and 1280 cm^{-1}. So, doubly deprotonated phosphate macrochelates present a less good agreement with the experimental IRMPD spectrum, and can be reasonably ruled out.

The structure of gaseous deprotonated monunucleotides has been investigated by spectroscopy techniques.[64-66] More particularly, Nei at al.[66] recently recorded the IRMPD spectrum of $(dGMP\text{-}H)^-$ from 600 to 1800 cm^{-1}. Comparison with DFT calculations points to a mixture of three *Syn* forms, the ribose moiety adopting a C3'-*endo* conformation. These structures appear to be rather compact due to the formation of an intramolecular hydrogen bond between the 2-amino group and the deprotonated phosphate moiety. Interestingly, *Syn* and *Anti* forms could be differentiated thanks to several experimental bands. Such distinction could not be achieved in presence of lead. One noticeable difference is the guanine C=O stretch, observed at 1715 cm^{-1} for $(dGMP\text{-}H)^-$. This mode is red-shifted by 45 cm^{-1} in presence of Pb^{2+}, further supporting the interaction of the metal with the guanine carbonyl group. Finally, like for $(dGMP\text{-}H)^-$, the comparison between IRMPD and DFT-computed

spectra supports the formation of a complex adopting in the gas phase a C3'-*endo* ribose conformation.

In summary, IRMPD experiments strongly suggest that gaseous $[Pb(dGMP-H)]^+$ ions adopt a macrochelate structure, in which Pb^{2+} interacts with both the phosphate group and the guanine residue moiety. The agreement is excellent with the three most stable forms obtained by our DFT study (**dGMPS10**, **dGMPA13** and **dGMPS9**).

3.4 Cross section measurements by ion mobility (IM-MS)

The geometry of representatives structures found by quantum chemistry calculations was extracted for both unfolded and macrochelate forms. The collision cross sections calculated for the major conformers are gathered in Table 3. Looking at the most stable conformers (macrochelates), it is remarkable that the rotation of guanine around the glycosidic bond formally permits the transition from *Anti* to *Syn* conformations while keeping the tetradentate coordination mode of Pb^{2+} with the exact same atoms. It is therefore not surprising that the predicted CCS is not so much altered between both conformations. However, all macrochelates CCS are predicted to be on average 12 to 15 $Å^2$ smaller than those of extended structures, corresponding to over 10% difference on average between expected CCS. Interestingly, this expected cross section gap is greater than the experimental uncertainty and therefore turns to be sufficient to be experimentally measured (see Supporting Information 5S).

Ion mobility measurements were therefore performed in order to discriminate between the two conformational families. The arrival time distribution of $[Pb(dGMP)-H]^+$ is essentially centered around a central peak (see Supporting Information, section 5S). The width of this highly dominant peak is consistent with a single family of conformations drifting through the tube. The average CCS corresponding to this single feature is calculated, as explained in the experimental section, from evolution of ion drift time with $\frac{1}{E}$ via linear regression (correlation coefficient 0.9997, standard error on slope less than 0.5%). The derived average CCS of $[Pb(dGMP)-H]^+$ is 99.6 $Å^2$ (calibration curve is

provided in Supporting Information, section 5S). The main sources of experimental uncertainties leading to error on Ω are temperature readout (~1%) and pressure readout and fluctuations (~3-4%), so that it is safe to consider Ω_{exp}=100± 5 $Å^2$, which is remarkably compact with regards to expected values (Table 3). Insterestingly, the structure of deprotonated dGMP has also been investigated by ion mobility[67] and a the experimental CCS (103±1 $Å^2$) is of the same order of magnitude as for $[Pb(dGMP)-H]^+$ complex. Such a value is again consistent with a compact form in the gas phase, and was assigned by comparison with molecular mechanics later confirmed by IRMPD spectroscopy[66], to the ribose being twisted into a C3'-*endo* conformation and guanine in *Syn* orientation, which allows the establishment of a hydrogen bond between the amino group and the deprotonated phosphate of the $(dGMP-H)^-$ anion. The most stable forms found for the metal complex, macrochelates, present the same type of ribose twist. Remarkably enough, despite the addition of lead the average CCS remains of the same order of magnitude as deprotonated dGMP. In the most stable structures, guanine and phosphate establish each a two-fold interaction to tetracoordinated lead, which is most likely responsible for the compactness of the structure.

The global conclusion from ion mobility experiments on $[Pb(dGMP)-H]^+$ is twofold: one single family of conformations is experimentally observed, and those conformations are compact. . CCS values obtained for macrochelates (folded structures) are in better agreement with the experimental value than unfolded forms. The mono-dispersity and compactness derived from mobility experiments suggest only macrochelate structures are populated in the gas phase, i.e. conformations where guanine folds (in either way, *Anti* or *Syn*) to provide additional coordination to Pb^{2+}. This observation is therefore in agreement with the analysis of IRMPD spectra.

IV-Conclusions/perspectives

The present study nicely illustrates how complementary experimental techniques can provide very detailed information about the structure of gaseous ions generated by electrospray. While MS/MS

experiments would suggest several possible coordination modes for the $[Pb(dGMP)-H]^+$ complex, both IRMPD spectroscopy and ion mobility experiments point to the gas-phase formation of macrochelates, in which Pb^{2+} ions simultaneously interacts with the deprotonated phosphate group and the guanine residue. Ion mobility data indicate that a single family of structures is generated in the gas phase and the IRMPD spectrum is in excellent agreement with macrochelates in which the metal, in addition to the phosphate group is coordinated to both the N7 and O6 position of guanine. Again, this particular interaction mode does not prevent the complexes from expelling the intact nucleobase under CID conditions. Consequently, losing the nucleobase does not necessarily mean a lack of interaction between the metal and the nucleobase moiety, as commonly mentioned during CID studies of oligonucleotides. Additional experiments are currently under progress with bigger oligonucleotides. Finally, the present study also demonstrates that the structure of $[Pb(dGMP)-H]^+$ in the gas phase differs from those deduced in solution from potentiometric studies.

Acknowledgements

The authors wish to thank the CLIO team (J. M. Ortega, C. Six, G. Perilhous, J. P. Berthet) as well as P. Maître and V. Steinmetz for their support during the experiments. JYS would like to thank the GDR 2758 “agregation, fragmentation et thermodynamique de systèmes moléculaires complexes isolés” for financial support. The research leading to these results has received funding from the European Research Council under the European Union's Seventh Framework Programme (FP7/2007-2013 Grant agreement N°320659).

Table and Figure caption

Figure 1: MS/MS spectra of the $[Pb(dGMP)-H]^+$ complex recorded with a collision energy of 25 eV (laboratory frame) and a DP parameter set to 40 V.

Figure 2: Relevant optimized structures of the $[Pb(dGMP)-H]^+$ complex. Relative free energies are given in kJ/mol.

Figure 3 : IRMPD spectrum (a) obtained for the $[Pb(dGMP)-H]^+$ complex compared to DFT-computed IR absorption spectra (b–f) of some relevant structures. The experimental IRPMD spectrum in overlayed in grey.

Table 1: Relative energies and structural features of the different structures optimized for the $[Pb(dGMP)-H]^+$ complex

Table 2: Experimental and computed IR vibrational bands for the $[Pb(dGMP)-H]^+$ complex

Table 3: theoretical collision cross sections calculated for representative possible conformations of the $[Pb(dGMP)-H]^+$ ion, and compared to the value deduced from drift tube ion mobility experiments.

Bibliography

1. K. O. Zhurov, L. Fornelli, M. D. Wodrich, U. A. Laskay and Y. O. Tsybin, *Chem. Soc. Rev.*, 2013, 42, 5014-5030.

2. J. E. P. Syka, J. J. Coon, M. J. Schroeder, J. Shabanowitz and D. F. Hunt, *PNAS*, 2004, 101, 9528-9533.

3. B. A. Budnik, K. F. Haselmann and R. A. Zubarev, *Chem. Phys. Lett.*, 2001, 342, 299-302.

4. R. Antoine, J. Lemoine and P. Dugourd, *Mass Spectrom. Rev.*, 2013, DOI: 10.1002/mas.21402, n/a-n/a.

5. D. E. Clemmer, R. R. Hudgins and M. F. Jarrold, *J. Am. Chem. Soc.*, 1995, 117, 10141-10142.

6. P. Dugourd, R. R. Hudgins, D. E. Clemmer and M. F. Jarrold, *Rev. Sci. Instrum.*, 1997, 68, 1122-1129.

7. D. E. Clemmer and M. F. Jarrold, *J. Mass Spectrom.*, 1997, 32, 577-592.

8. S. D. Pringle, K. Giles, J. L. Wildgoose, J. P. Williams, S. E. Slade, K. Thalassinos, R. H. Bateman, M. T. Bowers and J. H. Scrivens, *Int. J. Mass Spectrom.*, 2007, 261, 1-12.

9. A. B. Kanu, P. Dwivedi, M. Tam, L. Matz and J. Herbert H. Hill, *J. Mass Spectrom.*, 2008, 43, 1-22.

10. L. S. Fenn, M. Kliman, A. Mahsut, S. R. Zhao and J. A. McLean, *Anal. Bioanal.Chem.*, 2009, 394, 235-244.

11. L. MacAleese and P. Maître, *Mass Spectrom. Rev.*, 2007, 26, 583-605.

12. T. D. Fridgen, *Mass Spectrom. Rev.*, 2009, 28, 586-607.

13. M. K. Drayß, D. Blunk, J. Oomens, N. Polfer, C. Schmuck, B. Gao, T. Wyttenbach, M. T. Bowers and M. Schäfer, *Int. J. Mass Spectrom.*, 2009, 281, 97-100.

14. J. C. Poully, F. Lecomte, N. Nieuwjaer, B. Manil, J. P. Schermann, C. Desfrançois, G. Grégoire, R. Ballivian, F. Chirot, J. Lemoine, F. Calvo, R. Antoine and P. Dugourd, *Int. J. Mass Spectrom.*, 2010, 297, 28-35.

15. G. Papadopoulos, A. Svendsen, O. V. Boyarkin and T. R. Rizzo, *Faraday Discuss.*, 2011, 150, 243-255.

16. B. Bellina, I. Compagnon, L. MacAleese, F. Chirot, J. Lemoine, P. Maitre, M. Broyer, R. Antoine, A. Kulesza, R. Mitric, V. Bonacic-Koutecky and P. Dugourd, *Phys. Chem. Chem. Phys.*, 2012, 14, 11433-11440.

17. T. Le, J. Poully, F. Lecomte, N. Nieuwjaer, B. Manil, C. Desfrançois, F. Chirot, J. Lemoine, P. Dugourd, G. Rest and G. Grégoire, *J. Am. Soc. Mass Spectrom.*, 2013, 24, 1937-1949.

18. S. Zucker, S. Lee, N. Webber, S. Valentine, J. Reilly and D. Clemmer, *J. Am. Soc. Mass Spectrom.*, 2011, 22, 1477-1485.

19. S. Guillaumont, J. Tortajada, J. Y. Salpin and A. M. Lamsabhi, *Int. J. Mass Spectrom.*, 2005, 243, 279-293.

20. A. M. Lamsabhi, M. Alcamí, O. Mó, M. Yáñez, J. Tortajada and J.-Y. Salpin, *ChemPhysChem*, 2007, 8, 181-187.

21. C. Trujillo, A. M. Lamsabhi, O. Mó, M. Yáñez and J. Y. Salpin, *Org. Biomol. Chem.*, 2008, 6, 3695-3702.

22. J. Y. Salpin, S. Guillaumont, J. Tortajada and A. M. Lamsabhi, *J. Am. Soc. Mass Spectrom.*, 2009, 20, 359-369.

23. J.-Y. Salpin, L. Gamiette, J. Tortajada, T. Besson and P. Maître, *Int. J. Mass Spectrom.*, 2011, 304, 154-164.

24. J.-Y. Salpin, S. Guillaumont, D. Ortiz, J. Tortajada and P. Maître, *Inorg. Chem.*, 2011, 50, 7769-7778.

25. C. Trujillo, A. Lamsabhi, O. Mo, M. Yanez and J. Y. Salpin, *Int. J. Mass Spectrom.*, 2011, 306, 27-36.

26. B. Chiavarino, M. E. Crestoni, S. Fornarini, D. Scuderi and J. Y. Salpin, *J. Am. Chem. Soc.*, 2013, 135, 1445-1455.

27. J. M. Bakker, T. Besson, J. Lemaire, D. Scuderi and P. Maitre, *J. Phys. Chem. A*, 2007, 111, 13415-13424.

28. R. Prazeres, F. Glotin, C. Insa, D. A. Jaroszynski and J. M. Ortega, *Eur. Phys. J. D*, 1998, 3, 87-93.

29. J. Lemaire, P. Boissel, M. Heninger, G. Mauclaire, G. Bellec, H. Mestdagh, A. Simon, S. Le Caer, J. M. Ortega, F. Glotin and P. Maitre, *Phys. Rev. Lett.*, 2002, 89, 273002-273001.

30. J. S. Prell, J. T. O'Brien and E. R. Williams, *J. Am. Soc. Mass Spectrom.*, 2010, 21, 800-809.

31. F. Albrieux, F. Calvo, F. Chirot, A. Vorobyev, Y. O. Tsybin, V. Lepère, R. Antoine, J. Lemoine and P. Dugourd, *J. Phys. Chem. A*, 2010, 114, 6888-6896.

32. H. E. Revercomb and E. A. Mason, *Anal. Chem.*, 1975, 47, 970-983.

33. M. J. Frisch, G. W. Trucks, H. B. Schlegel, G. E. Scuseria, M. A. Robb, J. R. Cheeseman, V. G. Zakrzewski, J. J. A. Montgomery, T. Vreven, K. N. Kudin, J. C. Burant, J. M. Millam, S. S. Iyengar, J. Tomasi, V. Barone, B. Mennucci, M. Cossi, G. Scalmi, N. Rega, G. A. Petersson, H. Nakatsuji, M. Hada, M. Ehara, K. Toyota, R. Fukuda, J. Hasegawa, M. Ishida, T. Nakajima, Y. Honda, O. Kitao, C. Adamo, J. Jaramillo, R. Gomperts, R. E. Stratmann, O. Yazyev, J. Austin, R. Cammi, C. Pomelli, J. Ochterski, P. Y. Ayala, K. Morokuma, G. A. Voth, P. Salvador, J. J. Dannenberg, V. G. Zakrzewski, S. Dapprich, A. D. Daniels, M. C. Strain, O. Farkas, D. K. Malick, A. D. Rabuck, K. Raghavachari, J. B. Foresman, J. V. Ortiz, Q. Cui, A. G. Baboul, S. Clifford, J. Cioslowski, B. B. Stefanov, G. Liu, A. Liashenko, P. Piskorz, I.

Komaromi, R. L. Martin, D. J. Fox, T. Keith, M. A. Al-Laham, C. Y. Peng, A. Nanayakkara, M. Challacombe, P. M. W. Gill, B. Johnson, W. Chen, M. W. Wong, C. Gonzalez and J. A. Pople, Gaussian, Inc., Wallingford CT, Gaussian03, Revision C.02 edn., 2003.

34. C. Lee, W. Yang and R. G. Parr, *Physical Reviews B*, 1988, 37, 785-789.

35. A. D. Becke, *J. Chem. Phys.*, 1993, 98, 5648-5652.

36. W. Küchle, M. Dolg, H. Stoll and H. Preuss, *Mol. Phys.*, 1991, 6, 1945-1963.

37. M. D. Halls, J. Velkovski and H. B. Schlegel, *Theor. Chem. Acc.*, 2001, 105, 413-421.

38. M. D. Halls and H. B. Schlegel, *J. Chem. Phys.*, 1998, 109, 10587-10593.

39. *NIST Computational Chemistry Comparison and Benchmark Database. NIST Standard Reference Database Number 101* . Russell D. Johnson III 2005.

40. J. Y. Salpin, J. Tortajada, M. Alcamí, O. Mó and M. Yáñez, *Chem. Phys. Lett.*, 2004, 383, 561-565.

41. A. A. Shvartsburg and M. F. Jarrold, *Chem. Phys. Lett.*, 1996, 261, 86-91.

42. G. von Helden, M.-T. Hsu, N. Gotts and M. T. Bowers, *J. Phys. Chem.*, 1993, 97, 8182-8192.

43. G. von Helden, T. Wyttenbach and M. T. Bowers, *Int. J. Mass Spectrom. Ion Processes*, 1995, 146-147, 349-364.

44. M. F. Mesleh, J. M. Hunter, A. A. Shvartsburg, G. C. Schatz and M. F. Jarrold, *J. Phys. Chem.*, 1996, 100, 16082-16086.

45. C. Bleiholder, T. Wyttenbach and M. T. Bowers, *Int. J. Mass Spectrom.*, 2011, 308, 1-10.

46. E. T. I. Auteurs et Experts, in *Base documentaire*, Editions T.I., 2013, vol. tiaka.

47. C. P. Da Costa and H. Sigel, *J. Biol. Inorg. Chem.*, 1999, 4, 508-514.

48. M. T. Rodgers, S. A. Campbell and J. L. Beauchamp, *Int. J. Mass Spectrom. Ion Processes*, 1997, 161, 193-216.

49. Y. Xiang, Z. Abliz and M. Takayama, *J. Am. Soc. Mass Spectrom.*, 2004, 15, 689.

50. D. R. Phillips and J. A. McCloskey, *Int. J. Mass Spectrom. Ion Processes*, 1993, 128, 61-82.

51. C. P. Da Costa and H. Sigel, *Inorg. Chem.*, 2000, 39, 5985-5993.

52. H. Sigel, C. P. Da Costa and R. B. Martin, *Coord. Chem. Rev.*, 2001, 219, 435-461.

53. N. Russo, M. Toscano, A. Grand and F. Jolibois, *J. Comput. Chem.*, 1998, 19, 989-1000.

54. A. K. Chandra, M. T. Nguyen, T. Uchimaru and T. Zeegers-Huyskens, *J. Phys. Chem. A*, 1999, 103, 8853-8860.

55. Y. Podolyan, L. Gorb and J. Leszczynski, *J. Phys. Chem. A*, 2000, 104, 7346-7352.

56. O. Y. Ali and T. D. Fridgen, *Int. J. Mass Spectrom.*, 2011, 308, 167-174.

57. A. A. Power, O. Y. Ali, M. B. Burt and T. D. Fridgen, *Int. J. Mass Spectrom.*, 2012, 330, 233-240.

58. J. Oomens, B. G. Sartakov, G. Meijer and G. von Helden, *Int. J. Mass Spectrom.*, 2006, 254, 1-19.

59. C. F. Correia, P. O. Balaj, D. Scuderi, P. Maitre and G. Ohanessian, *J. Am. Chem. Soc.*, 2008, 130, 3359-3370.

60. D. T. Moore, J. Oomens, J. R. Eyler, G. von Helden, G. Meijer and R. C. Dunbar, *J. Am. Chem. Soc.*, 2005, 127, 7243-7254.

61. D. Schroder, H. Schwarz, P. Milko and J. Roithova, *J. Phys. Chem. A*, 2006, 110, 8346-8353.

62. J. R. Eyler, *Mass Spectrom. Rev.*, 2009, 28, 448-467.

63. B. Chiavarino, M. E. Crestoni, O. Dopfer, P. Maitre and S. Fornarini, *Angew. Chem. Int. Ed.*, 2012, 51, 4947-4949.

64. X. Yang, X.-B. Wang, E. R. Vorpagel and L.-S. Wang, *PNAS*, 2004, 101, 17588-17592.

65. Y. w. Nei, K. T. Crampton, G. Berden, J. Oomens and M. T. Rodgers, *The Journal of Physical Chemistry A*, 2013, 117, 10634-10649.

66. Y. w. Nei, N. Hallowita, J. D. Steill, J. Oomens and M. T. Rodgers, *J. Phys. Chem. A*, 2013, 117, 1319-1335.

67. J. Gidden and M. T. Bowers, *The Journal of Physical Chemistry B*, 2003, 107, 12829-12837.

Table 1: Relative energies and structural features of the different structures optimized for the $[Pb(dGMP)-H]^+$ complex

Structure[(a)]	Δ_0E_1[(b)]	$\Delta_{298}G_1$[(b)]	Δ_0E_2[(c)]	$\Delta_{298}G_2$[(c)]	Comments
dGMPA1	+383.7	+370.2	+378.4	+366.7	Zwitterionic
dGMPA2	+96.4	+84.4	+84.5	+74.3	Doubly deprot. phosphate, N7 protonated
dGMPA3	+96.6	+98.4	+104.7	+108.3	Doubly deprot. phosphate, N7 protonated
dGMPA4	+112.5	+100.4	+101.1	+90.8	Doubly deprot. phosphate, N7 protonated
dGMPA5	+164.7	+152.8	+153.5	+143.3	Doubly deprot. phosphate, O6 protonated
dGMPA6	+152.4	+140.0	+143.0	+132.4	Doubly deprot. phosphate, O6 protonated
dGMPA7	+197.2	+184.2	+184.9	+173.6	Doubly deprot. phosphate, N3 protonated
dGMPA8	+169.5	+160.4	+160.8	+153.4	
dGMPA9	+169.6	+156.9	+158.3	+147.3	
dGMPA10	+287.5	+267.3			
dGMPA11	+163.6	+152.7	+155.0	+145.9	
dGMPA12	+147.0	+136.0	+135.1	+125.9	
dGMPA13	0	0	0	+1.8	Macrochelate
dGMPS1	+395.2	+383.0			Zwitterionic
dGMPS2	+113.0	+113.1	+117.8	+119.6	Doubly deprot. phosphate, N7 protonated
dGMPS3	+166.2	+156.3	+152.7	+144.4	
dGMPS4	+129.8	+125.9	+128.5	+126.4	
dGMPS5	+167.6	+163.4	+164.0	+161.5	Macrochelate
dGMPS6	+123.4	+120.8	+131.6	+130.8	Macrochelate
dGMPS7	+81.2	+80.7	+83.8	+85.0	Macrochelate
dGMPS8	+72.5	+73.4	+72.2	+74.8	Macrochelate
dGMPS9	+13.0	+11.5	+9.2	+9.5	Macrochelate
dGMPS10	7.0	+4.4	+0.8	0	Macrochelate

(a) By convention, the *Syn* conformation (S) corresponds to a C4-N9-C'1-O4' torsional angle ranging from 0 to 90°. Otherwise, the conformation is *Anti* (A)

(b) Obtained at the B3LYP/6-31G(d,p) level, incl. ZPE or thermal corrections

(c) Obtained at the B3LYP/6-311+G(2df,2p)//B3LYP/6-31G(d,p) level, incl. ZPE or thermal corrections.

Table 2: Experimental and computed IR vibrational bands for the $[Pb(dGMP)-H]^+$ complex

Wavenumbers			DFT-computed intensities (km/mol)		Vibrational mode [(a)]
Exp.	Calc.		**dGMPA13**	**dGMPS10**	
	981		43		δ P–O–H
1000	986		90		δ P–O–H+δ C3'–O–H
	1008			169	ν P–O
1025-1150	1024			101	ν P–O + δ P–O–H
	1024		227		ν P–O
	1062		220		ν C5'–O4'
	1062			183	ν C5'–O5'
	1070			78	ν P–O
	1078		445		ν P–O
	1082		53		ν C3'–C4'
	1083			354	ν C3'–O3'
	1096			174	ν C1'–O4'
	1101		39		ν C3'–O3'
	1160		130		δ C8H
	1175			135	τ $C2'H_2$ + δ C8H
1165-1210	1184		56		ν C1'–N9 (guanine ring breathing)
	1195		80		δ C'–O'–H +δ C'–C'–H
	1205			101	δ C'–O'–H +δ C'–C'–H
1300-1340	1297			27	δ C'–C'–H
	1300		32		δ C'–C'–H+ δ N1H
	1301			41	δ C'–C'–H+ δ N1H
	1304		73		δ C'–C'–H+ δ N1H
	1318		24		δ C'–C'–H
	1343			70	ν C5-N7
	1380			59	ν C2-N1+ν C4=N9
1390	1381		59		ν C2-N1+ν C4=N9
	1397		33		δ C'–C3'–H
1586	1570		202		ν C4-C5
	1574			178	ν C4-C5
1625	1621			1091	δ NH_2 scissoring
	1621		1042		δ NH_2 scissoring
1670	1670		615		ν C6=O6
	1674			609	ν C6=O6

(a) Bond multiplicity as described by the NBO analysis

Table 3: theoretical collision cross sections calculated for representative possible conformations of the $[Pb(dGMP)-H]^+$ ion, and compared to the value deduced from drift tube ion mobility experiments.

Structure	Collision Cross Section (Å²)		
	PA *Pb=P=Si*	EHSS *Pb=P=Si*	Experiment
	Unfolded forms		
dGMPA1	114.7	121.5	
dGMPA2	115.5	122.7	
dGMPA12	117.5	124.9	
	Macrochelate forms		
dGMPA13	104.1	111.0	
dGMPS5	106.9	114.2	
dGMPS7	104.9	111.6	
dGMPS9	106.5	113.3	
dGMPS10	107.2	113.8	
			100 ± 5

Graphical abstract